



Subwavelength light confinement and enhancement enabled by dissipative dielectric nanostructures

KAICHEN DONG,^{1,2,3,†} YANG DENG,^{1,†} XI WANG,¹ KYLE B. TOM,^{1,2} ZHENG YOU,³ AND JIE YAO^{1,2,*}

¹Department of Materials Science and Engineering, University of California, Berkeley, California 94720, USA

²Materials Sciences Division, Lawrence Berkeley National Laboratory, Berkeley, California 94720, USA

³State Key Laboratory of Precision Measurement Technology and Instruments, Department of Precision Instrument, Tsinghua University, Beijing 100084, China

*Corresponding author: yaojie@berkeley.edu

Received 22 January 2018; revised 13 March 2018; accepted 15 March 2018; posted 15 March 2018 (Doc. ID 320196); published 11 April 2018

Dissipative loss in optical materials is considered one of the major challenges in nano-optics. Here we show that, counter-intuitively, a large imaginary part of material permittivity contributes positively to subwavelength light enhancement and confinement. The Purcell factor and the fluorescence enhancement of dissipative dielectric bowtie nanoantennas, such as Si in ultraviolet (UV), are demonstrated to be orders of magnitude higher than their lossless dielectric counterparts, which is particularly favorable in deep UV applications where metals are plasmonically inactive. The loss-facilitated field enhancement is the result of a large material property contrast and an electric field discontinuity. These dissipative dielectric nanostructures can be easily achieved with a great variety of dielectrics at their Lorentz oscillation frequencies, thus having the potential to build a completely new material platform boosting light-matter interaction over broader frequency ranges, with advantages such as bio-compatibility, CMOS compatibility, and harsh environment endurance. © 2018 Optical Society of America

OCIS codes: (310.6628) Subwavelength structures, nanostructures; (160.4670) Optical materials; (130.0130) Integrated optics.

<https://doi.org/10.1364/OL.43.001826>

Subwavelength light confinement and subwavelength light enhancement have greatly facilitated light-matter interaction, and they have led to a variety of applications in fields such as nonlinear optics, optical sensing, quantum information processing, nanolaser technology, and metrology [1–5]. Although plasmonics based on noble metals has been widely utilized to confine light to dimensions well below the diffraction limit [3–5], the intrinsic properties of noble metal systems lead to a number of limitations in their applications, such as plasmonic inactivity in UV range [6,7], bio-incompatibility [8,9], mechanical deformation, and thermal instabilities [10]. To overcome them, a variety of materials with negative permittivity bands, such as

semiconductors, graphene, and conductive oxides [11–13], have been investigated for plasmonic applications. In all of these materials, dissipative material loss, represented by the imaginary part of permittivity (ϵ_i), exists ubiquitously and has been widely believed to be detrimental for many applications. Research efforts so far have been focused on minimizing the material loss [13]. For example, dielectric structures with significantly smaller loss than metals have also been utilized to compress light into subwavelength structures [14–16]. However, those lossless dielectrics are unable to show comparable light enhancement capabilities as plasmonic structures [14,15].

Here, we show that, counter-intuitively, a large ϵ_i in dielectric nanostructures may contribute to field enhancement and field confinement effectively, and the small light enhancement factor (EF) in existing dielectric systems [14,15] can be greatly improved with the introduction of large material loss. We first analyze this phenomenon using widely investigated optical nanoantennas [17–19] as examples, which can bridge light fields at mismatched scales and realize electromagnetic (EM) confinement and EM enhancement in a deep subwavelength “hotspot.” The element Si is selected as our example because of its wide applications and its large dissipative loss at UV due to the interband transitions [20]. Specifically, amorphous Si (a-Si) [21] is utilized for easier potential experimental realization. We show that, compared with Au (noble metal), HfO_2 (lossless, high refractive index dielectric), and artificial lossy dielectrics with weaker Lorentz oscillation strength, the a-Si nanoantenna has a much stronger ability to confine and enhance UV light with a better Purcell factor and larger fluorescence enhancement. To understand that effect, light confinement in corresponding lossy nanogap structure models is analytically studied, which demonstrates quantitatively that the favorable light enhancement properties of the lossy dielectric antennas are due to larger dielectric discontinuities and an impedance mismatch.

A typical bowtie optical antenna used in our simulations (COMSOL Multiphysics) is depicted in Fig. 1(a), consisting of two tip-to-tip triangles separated by a small gap of

9 nm (G) [19]. The width (W), length (L), and thickness (T) of the bowtie are 115 nm, 53 nm, and 20 nm, respectively, and round tips with 11-nm radius (R) are used to imitate real fabrication. The bowtie is placed on a substrate (refractive index $n = 1.5$) in air ($n = 1$) and excited by an x-polarized EM wave along the $+z$ direction. Similar to the plasmonic bowtie antennas, the a-Si antenna has the overall amplitude EF greatly improved inside the gap [Fig. 1(b)]. Here, the amplitude/intensity EF is defined as the ratio of the local E-field amplitude/intensity, to the E-field amplitude/intensity at the same geometrical point without the bowtie in the simulation. In Fig. 1(c), the cross-sectional time-average EM energy density (TED) distribution of the Au bowtie [7] and the a-Si bowtie at 840 THz (3.5 eV) are shown as an example. The a-Si bowtie has a better performance for light confinement at this frequency.

It's illuminating to compare the a-Si, Au, Al [22], HfO_2 [23], and artificial dispersive dielectrics following similar but weaker Lorentz oscillation. The Lorentz oscillator model is given by

$$\tilde{\epsilon}(\omega) = \epsilon_{\infty} + \frac{(\epsilon_s - \epsilon_{\infty})\omega_t^2}{\omega_t^2 - \omega^2 + i\Gamma_0\omega}. \quad (1)$$

To make such artificial materials, ϵ_{∞} , ω_t , and Γ_0 are fixed to be 1.1, 890 THz, and 440 THz, respectively, while the static dielectric constant ϵ_s ($\epsilon_s = \epsilon_{\infty} + \omega_p^2/\omega_t^2$, ω_p is plasma frequency) is a tunable number as 2, 6, or 10. Thus, their frequency-dependent permittivities are similar to that of a-Si, as shown in Fig. 2(a), which also depicts the plasmonic inactivity of Au in UV. Note that when a-Si permittivity is fitted to with Eq. (1) by adjusting the involved parameters, the corresponding ϵ_s equals to 19.5.

Figure 2(b) shows the intensity EFs (calculated at the bowtie geometric center) as functions of the incident photon energy, demonstrating that the lossy a-Si bowtie achieves higher intensity enhancement than bowties made of Au and artificial materials. Also, the a-Si and Al bowties show comparable performance at higher frequencies. Ag is outperformed by Al in the UV range and is thus not discussed here for clarity [6]. All lossy dielectric bowties show similar enhancement behavior in all frequencies studied here and the EF increases by 10–20 folds over a broad range with larger ϵ_i . Most importantly, such a large enhancement is achieved in UV range, which is a long-term research aim in fields such as bioimaging and biosensing [24], due to plasmonic inactivity of noble metals in this region [6,7,25]. Even though Al has been considered

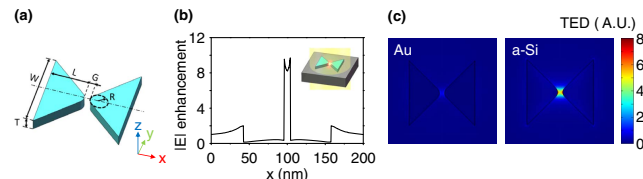


Fig. 1. Simulation of bowtie nanoantennas. (a) Geometry of the bowtie structure with the symmetry axis (represented as a dash-dot line) as the x -axis of the right-hand coordinate system. (b) Line scan of the E-field amplitude enhancement along the bowtie symmetry axis at half thickness at the working frequency of 840 THz. Inset: schematic of the simulated physical scenario. (c) The cross-sectional TED distribution of the Au bowtie antenna and the a-Si bowtie antenna with the same colorbar range.

as one solution [24], it possesses similar limits in deep UV [6] and other problems of cytotoxicity [9], severe oxidation [26,27], and device fabrication challenges when scaled down for short wavelength applications [28]. Therefore, our proposed lossy dielectrics overwhelm conventional materials (Au, Ag, Al, etc.) in those aspects [29], and they can be easily achieved in either UV or deep UV [20].

Mode volumes (V_{eff}) [30] and Purcell factors [30,31] are also computed in Fig. 2(c). Two orders of magnitude decrease in V_{eff} are achieved in lossy dielectric antennas with a larger ϵ_i , surpassing the widely accepted $V_{\text{eff}} \sim (\lambda/2)^3$ limit for the dielectric resonators [3] (λ is the EM field wavelength). A growing Purcell factor with an increasing ϵ_i verifies that better light confinement and the funneling of energy from the propagating light to the hotspot are achieved in lossy dielectric nanoantennas. The Purcell factor of the a-Si bowtie antenna is comparable to those of some metallic nanoantennas working in the visible range or even longer wavelengths [32,33].

Besides light confinement and light enhancement, device-level absorption loss has to be evaluated as compared to ϵ_i . Here, we introduce an “enhancement-loss figure of merit (FOM)” to evaluate those lossy dielectric bowties in Fig. 2(d), which is defined to be the ratio between the intensity EF and the total energy absorbed by an optical antenna. It is evident that a larger ϵ_i leads to a larger FOM, meaning light confinement with unit material absorption loss is boosted, and the FOM of the a-Si bowtie is 5 times that of the Au bowtie.

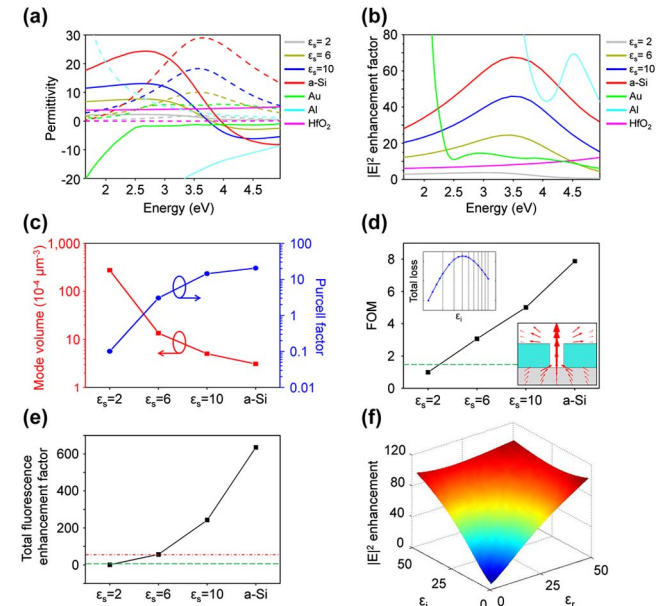


Fig. 2. Performance of lossy bowtie nanoantennas. (a) The permittivity of materials involved in the numerical calculation. The solid and dashed lines indicate ϵ_r and ϵ_i , respectively. (b) Intensity EF versus incident light energy for bowties made of the materials in (a). (c) Extracted mode volumes and Purcell factors. (d) FOM at 840 THz with the dashed line indicating the value of Au bowtie. Note that the values are normalized to the smallest one. Inset in (d): total loss versus ϵ_i (left), and schematic of local power flow around the gap of a highly lossy dielectric bowtie (right). (e) Calculated fluorescence EFs with the green dashed and red dash-dot lines indicating the values of Au and HfO_2 bowties, respectively. (f) Intensity EF plotted as a function of ϵ_r and ϵ_i .

The increase of the FOM by lossy dielectrics owes to the better enhancement as well as the limited total absorption loss. To clarify that, we plot the total absorption loss of a dielectric bowtie with a fixed real part of permittivity (ϵ_r) as a function of ϵ_i in the left inset of Fig. 2(d), showing that the total loss will first reach a maximum and then decrease with a larger ϵ_i , which can be explained by the competition between material absorption loss and an impedance mismatch. The total absorption loss first increases with the larger ϵ_i . However, as ϵ_i keeps rising, more EM energy is “compressed” into the gap, and less EM energy is coupled into the bowtie [right inset of Fig. 2(d)] because of the huge impedance mismatch between the lossy bowtie and its surroundings. Consequently, an ultra-lossy dielectric bowtie only generates limited heat (material absorption loss is assumed to be the only heat source in optical antennas [14]), which, along with other advantages including thermal stability and chemical resistivity [34], promises the practical application of robust lossy dielectric nanoantennas.

Lossy dielectric antennas show great potential in applications such as biomolecule fluorescence enhancement [19], where two processes are involved: pump excitation (already discussed above) and fluorescence emission. Since the pump wavelength and the emission wavelength are normally close to each other, they are both set to be 840 THz in the following analysis. To simulate fluorescence emission, a dipole source is placed at the bowtie center, and the far-field radiated power in absence and presence of the bowtie are examined [19]. The radiated and non-radiated power EFs (normalized to the far-field radiated power in absence of bowtie antennas by definition) are calculated to obtain the quantum efficiency EF with the assumption that the intrinsic quantum efficiency of the sample is 2.5% [19]. The total fluorescence EF [Fig. 2(e)] is evaluated by multiplying the EF of pump excitation intensity with the quantum efficiency EF. The large ϵ_i of the a-Si bowtie leads to improvement in both radiative and non-radiative EFs, resulting in a total fluorescence EF of 636, much larger than those of the Au antenna (8) and the HfO₂ antenna (75), indicating its great potential in UV applications such as fluorescence detection from Tryptophan in proteins, which has been very troubling due to plasmonic inactivity in the UV or the oxidation of metals [35].

In general, ϵ_i contributes as much as ϵ_r to the impedance mismatch, hence the enhancement. As shown in Fig. 2(f), the intensity EF increases monotonically with the absolute value of permittivity ($|\epsilon|$) near the zero point, consistent with both the above analysis and analytical results in the following section. Previous application of large permittivity materials for subwavelength confinement faced great challenges to solely obtain a large ϵ_r , while in real materials, a large ϵ_r is always associated with a large loss. Our justification of the role of a large ϵ_i in nanoantennas solved the problem, allowing a new paradigm of material selection in subwavelength light confinement and light enhancement applications. Since a large ϵ_i is much easier to experimentally achieve than a large ϵ_r , the contribution of ϵ_i is even more effective in practice. Note that the saturation effect in Fig. 2(f), where $|\epsilon|$ is very large, owes to the compression of almost all the EM energy to the gap or the edge by impedance mismatch, and a greater mismatch makes no substantial difference.

To provide further insight into the contribution of loss to light confinement and light enhancement in dielectric

antennas, we analytically explore a simplified structure, i.e., a dielectric nanogap structure (NGS), consisting of two identical single-mode optical slabs separated by a small gap and surrounded by a bulk material [Fig. 3(a)] [15,16]. The complex permittivity distribution is

$$\epsilon(x) = \begin{cases} \epsilon_1, & |x| \leq a \\ \epsilon_{2r} + i\epsilon_{2i}, & a < |x| \leq b \\ \epsilon_3, & b < |x| < \infty \end{cases}, \quad (2)$$

where ϵ_1 , ϵ_{2r} , and ϵ_3 are real parts of permittivity, and ϵ_{2i} denotes the imaginary part of permittivity in the slabs (ϵ_2).

For the NGS, the electric field is polarized across the gap, with a y -polarized magnetic field, and x -polarized and z -polarized electric field components (TM mode) [15,16]. Here, we obtain the field distribution with the existence of strong material loss by combining the boundary conditions with the wave equation and solving the characteristic dispersion relation [15]. The ratio between the values of $|E_x|$ at the two sides of the interface equals to $[\epsilon_{2r}^2 + \epsilon_{2i}^2]^{1/2}/\epsilon_1$ across the interface. The permittivity contrast can be enlarged by introducing a larger loss (ϵ_{2i}), which is experimentally more practical than simply looking for a large ϵ_r .

An analytical three-dimensional (3D) spatial distribution of E_x for a symmetric fundamental mode (TM) at 840 THz is given in Fig. 3(b) and Fig. 3(c) in two different scenarios: without loss ($\epsilon_2 = 10 + 0i$) and with loss ($\epsilon_2 = 10 + 30i$). Here, we assume that $\epsilon_1 = \epsilon_3 = 1$, $a = 5$ nm, and $b = 55$ nm. As depicted in Fig. 3(c), the E_x inside the gap at the NGS entrance is amplified with the introduction of loss. Although E_x decays in the propagation direction [the cross-sectional plane in Fig. 3(a)], can be utilized to compress and enhance the optical field in subwavelength scale volumes. It is geometrically similar to typical nanoantennas, without substantial influence from the propagation decay. In Fig. 3(d), we depict the normalized E_x distribution in the plane of $z = 0$, which again shows the positive influence of

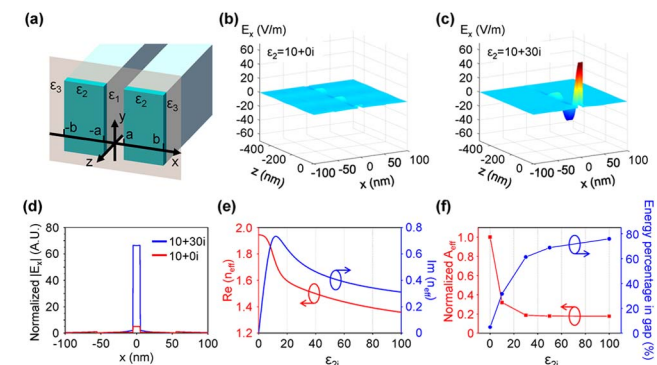


Fig. 3. E_x field distribution and performance of NGS. (a) Schematic of NGS infinitely long in the y direction. The shaded plane depicts the thin slice used in (d). The light propagates along the $-z$ direction. (b), (c) Analytically calculated 3D mapping of the field in NGS without loss (b) and with loss (c). (d) E_x spatial distribution along x -axis at the interface of $z = 0$. (e) Real and imaginary parts of n_{eff} plotted as functions of ϵ_{2i} . (f) The effective mode area of NGSs and energy percentage in the gap plotted as functions of ϵ_{2i} . The effective mode areas are normalized to the lossless case.

loss. Note that the above values of the calculated E_x are normalized to the ones at $|x| = b$ (in the air).

We further calculate the effective refractive index (n_{eff}) for more details about the propagation and field distribution, and plot the results as functions of ϵ_{2i} in Fig. 3(e). The imaginary part of n_{eff} first increases and then decreases when ϵ_{2i} goes up. This effect can also be explained by the competition between the field distribution and the increasing impedance mismatch by larger loss. In other words, the material loss not only enhances the field, but also eventually leads to less absorption loss and dissipation of energy.

To verify the subwavelength light confinement in NGSs, we calculate the cross-sectional mode area ($A_{\text{eff}} = \iint W dA / W_{\text{max}}$, W is energy density, and W_{max} is the maximum energy density in the cross section of NGS). Figure 3(f) shows the simulated dependence of A_{eff} on the loss (ϵ_{2i}). With an increasing ϵ_{2i} , the energy of the EM field is effectively compressed from the slabs into the gap, confirmed by the decreasing A_{eff} and the increasing energy percentage inside the gap, which goes up from $\sim 5\%$ to $\sim 78\%$ as ϵ_{2i} increases from 0 to 100, highlighting the great potential of the loss-induced energy confinement. That light confinement is also attributed to the impedance mismatch and the field discontinuities across the interface between the lossy slabs and the gap. These two mechanisms provide a clear explanation of the physics behind.

In summary, we demonstrated and analyzed large subwavelength light confinement and light enhancement inside dissipative dielectric nanostructures with the counter-intuitive contribution from ϵ_i , leading to a plethora of new materials suitable for nanophotonic applications. In agreement with the NGS model, loss helps create a large dielectric discontinuity and impedance mismatch at the material boundaries and, therefore, greatly boosts the EM field intensity in the nanostructure hotspots. As an example, a lossy dielectric nanoantenna made of a-Si displays remarkable light-matter interaction performance in the UV range with a Purcell factor and fluorescence enhancement larger than those of Au antennas and HfO_2 antennas. Such lossy dielectrics are easy to achieve using a Lorentz oscillator model with large ϵ_r and ϵ_i almost simultaneously in multiple frequencies, providing a better option when other material systems fail to achieve enough performance. For example, in deep UV where Al is already inactive, lossy dielectrics such as SiO_2 [36] and SiC [37] still work, with bio-compatibility [38,39], CMOS compatibility, and harsh environment endurance. Furthermore, based on the interband absorption-induced large ϵ_i , engineering the bandstructure of the material will enable great tunability in the working frequency of those devices. This finding paves the way towards a completely new category of optical devices based on dissipative dielectrics, which will further enrich the ways nanophotonic research is done and enable future large-scale applications that do not exist today.

Funding. National Science Foundation (NSF) (1555336); China Scholarship Council (CSC) (201406210211).

Acknowledgment. The authors acknowledge Professor Junqiao Wu, Professor Ming C. Wu, and Shuai Lou for helpful discussions.

[†]These authors contributed equally to this Letter.

REFERENCES

1. K. J. Vahala, *Nature* **424**, 839 (2003).
2. J. A. H. Van Nieuwstadt, M. Sandtke, R. H. Harmsen, F. B. Segerink, J. C. Prangsma, S. Enoch, and L. Kuipers, *Phys. Rev. Lett.* **97**, 146102 (2006).
3. J. A. Schuller, E. S. Barnard, W. Cai, Y. C. Jun, J. S. White, and M. L. Brongersma, *Nat. Mater.* **9**, 193 (2010).
4. D. K. Gramotnev and S. I. Bozhevolnyi, *Nat. Photonics* **4**, 83 (2010).
5. M. P. Nielsen, X. Shi, P. Dicht, S. A. Maier, and R. F. Oulton, *Science* **358**, 1179 (2017).
6. G. H. Chan, J. Zhao, G. C. Schatz, and R. P. V. Duyne, *J. Phys. Chem. C* **112**, 13958 (2008).
7. P. B. Johnson and R. W. Christy, *Phys. Rev. B* **6**, 4370 (1972).
8. S. M. Hussain, L. K. Braydich-Stolle, A. M. Schrand, R. C. Murdock, K. O. Yu, D. M. Mattie, J. J. Schlager, and M. Terrones, *Adv. Mater.* **21**, 1549 (2009).
9. D. L. Jones and L. V. Kochian, *FEBS Lett.* **400**, 51 (1997).
10. A. Kuhlicke, S. Schietinger, C. Matyssek, K. Busch, and O. Benson, *Nano Lett.* **13**, 2041 (2013).
11. U. Guler, V. M. Shalaev, and A. Boltasseva, *Mater. Today* **18**(4), 227 (2015).
12. U. Guler, A. Boltasseva, and V. M. Shalaev, *Science* **344**, 263 (2014).
13. P. R. West, S. Ishii, G. V. Naik, N. K. Emani, V. M. Shalaev, and A. Boltasseva, *Laser Photon. Rev.* **4**, 795 (2010).
14. M. Calderola, P. Albelia, E. Cortés, M. Rahmani, T. Roschuk, G. Grinblat, R. F. Oulton, A. V. Bragis, and S. A. Maier, *Nat. Commun.* **6**, 7915 (2015).
15. V. R. Almeida, Q. Xu, C. A. Barrios, and M. Lipson, *Opt. Lett.* **29**, 1209 (2004).
16. Q. Xu, V. R. Almeida, R. R. Panepucci, and M. Lipson, *Opt. Lett.* **29**, 1626 (2004).
17. N. Yu, E. Cubukcu, L. Diehl, D. Bour, S. Corzine, J. Zhu, G. Höfler, K. B. Crozier, and F. Capasso, *Opt. Express* **15**, 13272 (2007).
18. A. Alù and N. Engheta, *Phys. Rev. Lett.* **101**, 043901 (2008).
19. A. Kinkhabwala, Z. Yu, S. Fan, Y. Avlasevich, K. Müllen, and W. E. Moerner, *Nat. Photonics* **3**, 654 (2009).
20. G. E. Jellison, *Opt. Mater.* **1**, 41 (1992).
21. Taken from SOPRA N&K Database.
22. A. D. Rakic, *Appl. Opt.* **34**, 4755 (1995).
23. D. Franta, I. Ohlídal, D. Nečas, F. Vižd'a, O. Caha, M. Hasoň, and P. Pokorný, *Thin Solid Films* **519**, 6085 (2011).
24. M. Kikawada, A. Ono, W. Inami, and Y. Kawata, *Appl. Phys. Lett.* **104**, 223703 (2014).
25. S. Kawata, Y. Inouye, and P. Verma, *Nat. Photonics* **3**, 388 (2009).
26. L. Li, S. F. Lim, A. A. Puretzky, R. Riehn, and H. D. Hallen, *Appl. Phys. Lett.* **101**, 113116 (2012).
27. M. W. Knight, N. S. King, L. Liu, H. O. Everitt, P. Nordlander, and N. J. Halas, *ACS Nano* **8**, 834 (2014).
28. J. Martin and J. Plain, *J. Phys. D* **48**, 184002 (2015).
29. F. Erogogbo, K. T. Yong, I. Roy, R. Hu, W. C. Law, W. Zhao, H. Ding, F. Wu, R. Kumar, M. T. Swihart, and P. N. Prasad, *ACS Nano* **5**, 413 (2010).
30. S. Zhang, Y. S. Park, Y. Liu, T. Zentgraf, and X. Zhang, *Opt. Express* **18**, 6048 (2010).
31. E. M. Purcell, *Phys. Rev.* **69**, 681 (1946).
32. D. Arbel, N. Berkovitch, A. Nevet, A. Peer, S. Cohen, D. Ritter, and M. Orenstein, *Opt. Express* **19**, 9807 (2011).
33. C. Belacel, B. Habert, F. Bigourdan, F. Marquier, J. P. Hugonin, S. Michaelis de Vasconcellos, X. Lafosse, L. Coolen, C. Schwob, C. Javaux, B. Dubertret, J. J. Greffet, P. Senellart, and B. Dubertret, *Nano Lett.* **13**, 1516 (2013).
34. Y. T. Yang, K. L. Ekinci, X. M. H. Huang, L. M. Schiavone, M. L. Roukes, C. A. Zorman, and M. Mehregany, *Appl. Phys. Lett.* **78**, 162 (2001).
35. I. T. Chen, P. H. Chang, Y. C. Chang, and T. F. Guo, *Sci. Rep.* **3**, 1505 (2013).
36. R. Kitamura, L. Pilon, and M. Jonasz, *Appl. Opt.* **46**, 8118 (2007).
37. S. Zollner, J. G. Chen, E. Duda, T. Wetteroth, S. R. Wilson, and J. N. Hilfiker, *J. Appl. Phys.* **85**, 8353 (1999).
38. D. Tarn, C. E. Ashley, M. Xue, E. C. Carnes, J. I. Zink, and C. J. Brinker, *Acc. Chem. Res.* **46**, 792 (2013).
39. J. Botsoa, V. Lysenko, A. Géloën, O. Marty, J. M. Bluet, and G. Guillot, *Appl. Phys. Lett.* **92**, 173902 (2008).